

1 A high-spatial resolution soil carbon and nitrogen dataset for the
2 northern permafrost region, based on circumpolar land cover
3 upscaling

4

5

6 Juri Palmtag¹, Jaroslav Obu², Peter Kuhry^{3,4}, Andreas Richter⁵, Matthias B. Siewert⁶, Niels Weiss⁷;
7 Sebastian Westermann² and Gustaf Hugelius^{3,4}

8 ¹Department of Human Geography, Stockholm University, Stockholm, Sweden; ²University of Oslo,
9 Department of Geosciences, Sem Sælands vei 1, 0316 Oslo, Norway; ³Department of Physical Geography,
10 Stockholm University, Stockholm, Sweden; ⁴Bolin Centre for Climate Research, Stockholm University,
11 Stockholm, Sweden; ⁵Centre for Microbiology and Environmental Systems Science, University of Vienna,
12 Vienna; ⁶Department of Ecology and Environmental Science, Umeå University, Umeå, 901 87, Sweden;
13 ⁷Northwest Territories Geological Survey, Government of the Northwest Territories, Yellowknife NT X1A
14 1K3, Canada.

15

16 Corresponding author: Juri Palmtag (juri.palmtag@humangeo.su.se)

17

18

19

20

21

22 **Abstract**

23 Soils in the northern high latitudes are a key component in the global carbon cycle; the northern permafrost region
24 covers 22% of the Northern Hemisphere land surface area and holds almost twice as much carbon as the atmosphere.
25 Permafrost soil organic matter stocks represent an enormous long-term carbon sink which is in risk of switching to a
26 net source in the future. Detailed knowledge about the quantity and the mechanisms controlling organic carbon storage
27 is of utmost importance for our understanding of potential impacts of and feedbacks on climate change. Here we
28 present a geospatial dataset of physical and chemical soil properties calculated from 651 soil pedons encompassing
29 more than 6500 samples from 16 different study areas across the northern permafrost region. The aim of our dataset
30 is to provide a basis to describe spatial patterns in soil properties, including quantifying carbon and nitrogen stocks.
31 There is a particular need for spatially distributed datasets of soil properties, including vertical and horizontal
32 distribution patterns, for modelling at local, regional or global scales. This paper presents this dataset, describes in
33 detail soil sampling, laboratory analysis and derived soil geochemical parameters, calculations and data clustering.
34 Moreover, we use this dataset to estimate soil organic carbon and total nitrogen storage estimates in soils in the
35 northern circumpolar permafrost region ($17.9 \times 10^6 \text{ km}^2$) using the ESA's Climate Change Initiative (CCI) Global
36 Land Cover dataset at 300 m pixel resolution. We estimate organic carbon and total nitrogen stocks on a circumpolar
37 scale (excluding Tibet) for the 0-100 cm and 0-300 cm soil depth to be 380 Pg and 813 Pg for carbon and 21 Pg and
38 55 Pg for nitrogen, respectively. Our organic carbon estimates agree with previous studies, with most recent estimates
39 of 1000 Pg (-170 to $+186$ Pg) to 300 cm depth. Two separate datasets are freely available on the Bolin Centre Database
40 repository. Dataset references and DOIs are presented in the "Data access" section in the end.

41 **1. Introduction**

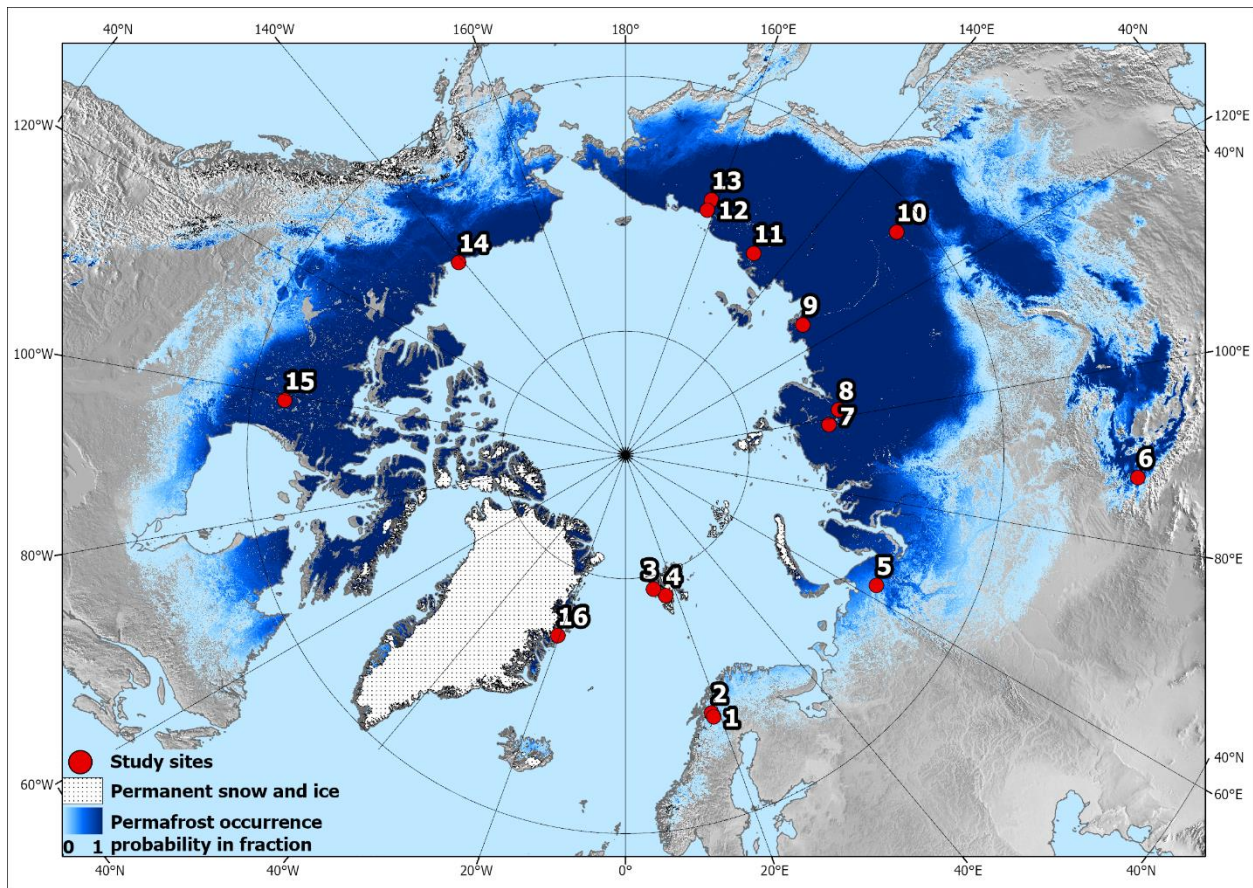
42 Permafrost soils represent a large part of the terrestrial carbon reservoir and form a significant and climate-sensitive
43 component of the global carbon cycle (Hugelius et al., 2014). High-latitude ecosystems are experiencing rapid climate
44 change causing warming of the soil, thawing of permafrost, and fluvial and coastal erosion (Biskaborn et al., 2019;
45 Fritz et al., 2017). Warming enhances the decomposition of organic matter (OM) by microorganisms, which produces
46 carbon dioxide, methane, and nitrous oxide. The release of these greenhouse gases to the atmosphere would in turn
47 generate further climate change, resulting in a positive feedback on global warming (Turetsky et al., 2020). To better
48 predict the magnitude and effect of environmental changes in the permafrost region, improved data on the properties
49 and quantities of carbon and nitrogen stored in these climate vulnerable soils are needed.

50 In many cases, a lack of observational data for parameterization or evaluation can limit model development or accurate
51 model projections (Flato, 2011). Soil properties such as OM content, soil texture and soil moisture or their derivatives
52 are commonly used to parametrize, train or validate models (e.g. Oleson et al., 2010). Yet, the representation of
53 northern soil profiles in global datasets remains limited (Köchy et al., 2015; Batjes, 2016), the northern circumpolar
54 permafrost region ($20.6 \times 10^6 \text{ km}^2$) in which permafrost can occur accounts for 22% of the Northern Hemisphere
55 exposed land area (Obu et al, 2019).

56 Many previous studies have shown a robust relationship between land cover and soil organic carbon (SOC)
57 distribution, making land cover datasets useful for upscaling estimates from soil profiles to full landscape coverage
58 (e.g. Kuhry et al., 2002; Hugelius, 2012; Palmtag et al., 2015; Siewert et al., 2015; Wojcik et al., 2019). Here we
59 describe the compilation of a harmonized soil dataset for permafrost-affected landscapes derived from 15 different
60 high latitude sites and one high alpine study site in Canada, Greenland, Svalbard, Sweden, and Russia (Fig. 1; Table
61 1). In total, 651 soil pedons contain information from up to 6529 samples on carbon and nitrogen content, carbon to
62 nitrogen (C/N) ratio, isotopic composition, texture (sand, silt + clay) and coarse fraction content, land cover type, wet
63 and dry bulk density, calculated volumetric contents for ice/water, and volumetric content of organic soil material,
64 mineral soil material and air. Site data were upscaled to the northern circumpolar permafrost region using the European
65 Space Agency (ESA) Climate Change Initiative (CCI) Global Land Cover dataset at 300 m pixel resolution, which is
66 the very first long-term global land cover time series product.

67 This study has two main aims. Firstly, the primary aim of this dataset is to provide a harmonized, high resolution,
68 quality controlled, and contextualized soil pedon dataset with a focus on SOC, nitrogen and other parameters essential
69 to determine the role of northern permafrost region soils in the climate system. Particularly, the extensive metadata
70 on soil properties included for many samples when available (texture, volumetric densities, active layer depth, ice
71 content, isotopic composition, etc.) are of great importance and can be used to identify and model the processes
72 responsible for the current and future carbon balance. Secondly, we used this soil dataset and an existing spatial
73 product for upscaling to provide a new and independent estimate of the SOC and total nitrogen (TN) storage estimates
74 within the northern circumpolar permafrost region.

75



76

77 Figure 1: Overview map with location of the 16 sampling sites (see Table 1). Blue shading indicates permafrost
 78 probability (dark hues showing higher permafrost occurrence probability), based on an equilibrium state model for
 79 the temperature at the top of the permafrost (TTOP) for the 2000–2016 period (Obu et al., 2019). North Pole Lambert
 80 azimuthal equal area projection (datum: WGS 84). Base map: Made with Natural Earth.

81

82 2.Methods

83 2.1 Dataset structure

84 The dataset contains 6529 analyzed samples from 651 soil pedons in 16 different sampling locations across the
 85 northern permafrost region (Fig 1; Table 1) (Palmtag et al., 2022a, b). Each sampled pedon was described and
 86 classified according to land cover type. Land cover is defined as the biophysical cover of the Earth's terrestrial surface
 87 such as different vegetation types, water, and bare ground.

88

89 Table 1: Summary of all study sites

Nr.	Study area	Country	Long	Lat	n=pedons	Reference
1	Tarfala	Sweden	18.63° E	67.91° N	55	Fuchs et al., 2015
2	Abisko	Sweden	18.05° E	68.33° N	125	Siewert, 2018
3	Ny Ålesund	Norway	11.83° E	78.93° N	28	Wojcik et al., 2019
4	Adventdalen	Norway	16.04° E	78.17° N	48	Weiss et al., 2017
5	Seida, Usa River Basin	Russia	62.55° E	67.35° N	44	Hugelius et al., 2009; 2011
6	Aktru, Altai mountains	Russia	87.47° E	50.05° N	39	Pascual et al., 2020
7	Logata, Taymyr	Russia	98.42° E	73.43° N	31	Palmtag et al., 2016
8	Arymas, Taymyr	Russia	101.90° E	72.47° N	35	Palmtag et al., 2016
9	Lena Delta	Russia	126.22° E	72.28° N	56	Siewert et al., 2016
10	Spasskaya Pad	Russia	129.46° E	62.25° N	33	Siewert et al., 2015
11	Tjokurdach	Russia	147.48° E	70.83° N	27	Siewert et al., 2015; Weiss et al., 2016
12	Shalaurovo	Russia	161.55° E	69.32° N	22	Palmtag et al., 2015
13	Cherskiy	Russia	161.30° E	68.45° N	15	Palmtag et al., 2015
14	Herschel Island	Canada	139.09° W	69.58° N	42	Siewert et al., 2021
15	Tulemalu Lake	Canada	99.16° W	62.55° N	16	Hugelius et al., 2010
16	Zackenbergl	Greenland	20.50° W	74.45° N	35	Palmtag et al., 2015; 2018

90

91 Land cover products are commonly satellite derived and sometimes globally available. We opted for a two-tier
 92 approach, where more classes can be used in products with higher thematic or spatial resolution (Table 2). First, we
 93 differentiated land cover into 5 primary tier classes (Tier I) which represent the major land cover types: forest, tundra,
 94 wetland, barren, and Yedoma. Although Yedoma is a sedimentary deposit and not a typical land cover class, it was
 95 added due to its large areal extent, special soil organic matter (SOM) and ground ice properties, as well as soil
 96 characteristics (Strauss et al., 2017; Weiss et al., 2016). Subsequently, Tier I classes were subdivided into 10 Tier II
 97 subclasses (Table 2).

98

99 Table 2: Hierarchical structure of the two-tier land cover class system applied to the pedons based on field
 100 observations.

TIER I		TIER II	
1	Forest	1.1	Deciduous broadleaf forest
		1.2	Evergreen needleleaf forest
		1.3	Deciduous needleleaf forest
2	Tundra	2.1	Shrub tundra
		2.2	Graminoid / forb tundra
3	Wetland	3.1	Permafrost wetlands
		3.2	Non-permafrost wetlands
4	Barren	4.1	Barren
5	Yedoma	5.1	Yedoma tundra
		5.2	Yedoma forest

101 **2.1.1 Class definitions of soil pedons to land cover types**

102 All sampling sites were classified with Tier I descriptions using field descriptions and, where possible, assigned a
 103 more detailed (Tier II) description. The forest class was used for sparse to dense forests, further separated into three
 104 different Tier II classes: deciduous broadleaf, evergreen needleleaf and deciduous needleleaf forest. Tundra is
 105 separated in Tier II to shrub tundra (dominated by erect shrubs > 50 cm height) and graminoid / forb tundra (with low
 106 growth heath vegetation or graminoid dominated). Wetland includes terrain that is saturated with water for sufficient
 107 time of the year to promote aquatic soil processes with low oxygen conditions and occurrence of vegetation fully
 108 adapted to these conditions, as well as all types of peatlands. Areas that met the National Wetlands Working Group
 109 (1997) definition of a wetland were classified as such. The permafrost status within the top 2 m of a site was used to
 110 distinguish in Tier II the permafrost wetlands and the non-permafrost wetlands. Although a substantial part of the
 111 northern circumpolar permafrost region is classified as water (0.98×10^6 km²) or permanent snow/ice (0.06×10^6 km²),
 112 no soil sample or pedon data from these classes are included in the database. The Tibetan permafrost region was also
 113 excluded from our estimates as none of the sampling sites originated from that area. The class barren includes land
 114 cover types such as exposed bedrock, boulder fields, talus slopes, debris cones, rock glaciers, where soil is either
 115 almost completely absent, or occurs only in minor patches (<10 % area) or in between boulders. The land cover class
 116 Yedoma is defined as areas in Siberia, Alaska, and Yukon underlain by late Pleistocene ice-rich syngenetic permafrost
 117 deposits. We used the spatial extent for the Yedoma domain from Strauss et al. (2017) which occupied an area of
 118 570,000 km² from the used ESA CCI land cover product. Tier II divides the Yedoma domain into Yedoma tundra and
 119 Yedoma forest.

120 2.2 Soil sampling

121 Field soil sampling took place in summer months (late June to early September) between 2006 and 2019, most
122 frequently in August or September in order to capture the maximum seasonal thaw (active layer) depth at each site.
123 Active layer thickness was measured at each location using a graduated steel probe or measuring tape in excavated
124 soil pits. A stratified sampling scheme consisting of linear transects with predefined equidistant intervals of typically
125 100 to 200 m across all major landscape elements was used to retrieve soil pedons ($n = 582$), with on average 37
126 sampling sites per study area. To ensure that this sampling scheme covered all representative landscape units and
127 types, maps (including vegetation, surficial geology) and remote sensing products (including air photos, satellite
128 imagery, and elevation models) were assessed prior to fieldwork. Detailed field reconnaissance involving visual
129 observation of the manageable study area were conducted before establishing transects. Sampling sites were located
130 and marked at the exact position based on distance to the first sampling point and compass bearing using a hand-held
131 GPS device. This ensured an unbiased location of individual sampling sites. When sufficient time was available in the
132 field, additional sampling ($n = 69$) using a random or stratified random distribution of sampling points was used.
133 Following the field sampling protocol (Figure S1), a site description, soil and in several cases phytomass sampling
134 were conducted at each sampling point.

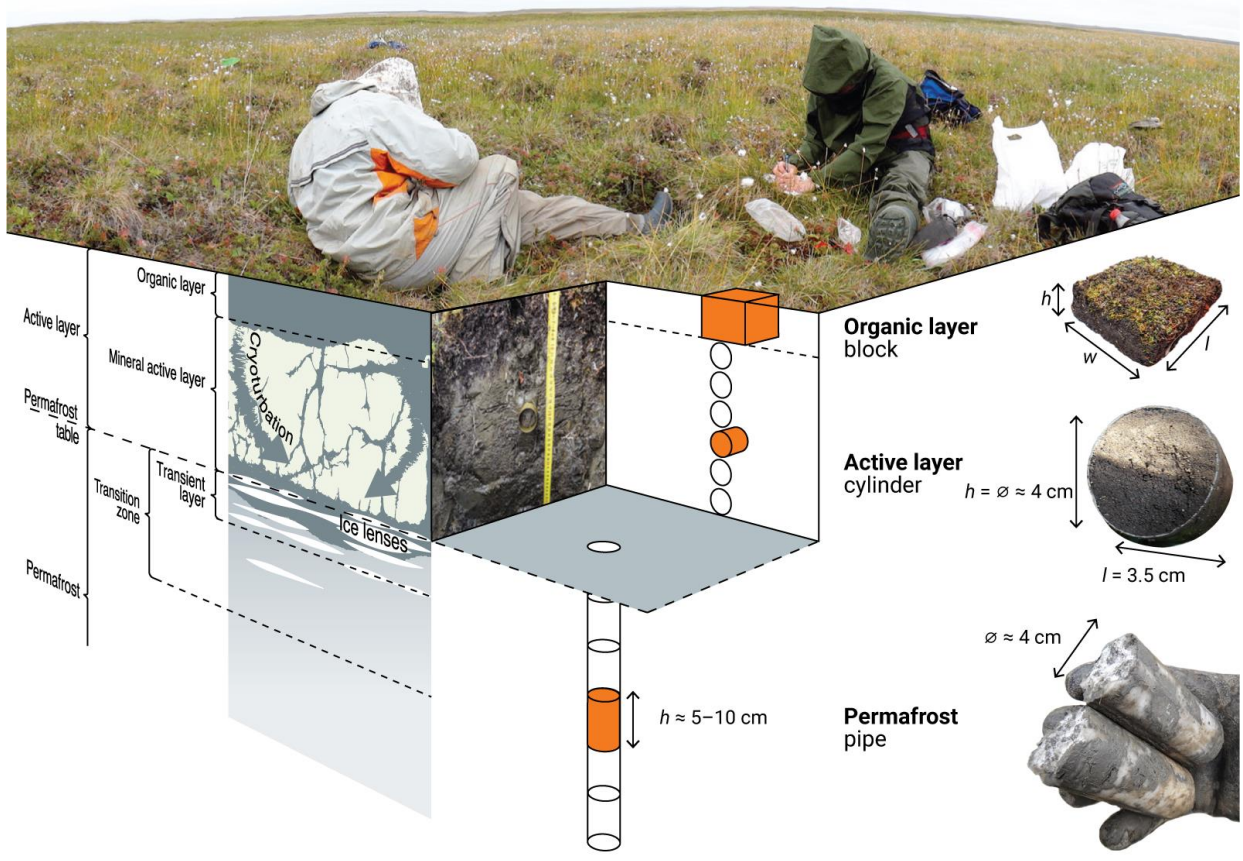
135 For each pedon, the organic layer and the active layer was sampled from an open soil pit excavated to the bottom of
136 the active layer, to the bedrock or when this was not possible, to a depth of at least 50 cm (Fig. 2). Deeper unfrozen
137 soil layers were sampled using a steel pipe (see permafrost sampling below). The organic layer sample was cut out as
138 a block using a pair of scissors or a knife (removing living vegetation), and the block volume was measured in the
139 field. The active layer samples were collected using 100 cm³ soil sampling rings inserted horizontally into the soil
140 profile. Sampling of the active layer was performed in fixed depth intervals (5–10 cm) or along soil horizon
141 boundaries. For non-permafrost wetland sites, a Russian peat corer with a 50 cm long chamber was used. After
142 extraction, the core was subdivided into smaller increments (generally 5 cm) which resulted typically in about 5–15
143 samples per sampling site depending on the reached depth.

144 The permafrost section of the soil profile and very deep unfrozen soil layers were sampled using a steel pipe that was
145 hammered into the ground in short (5 to 10 cm) depth increments. The pipe was pulled out after each sampled
146 increment using large pipe wrenches, and the sample was pushed out of the pipe using a steel rod. At several locations
147 ($n = 18$) permafrost samples were also collected from exposures along lake shores or river valleys where the steel pipe
148 was hammered in horizontally. These steel pipes are industry standardized with an outer diameter of 42.2 mm (1.25
149 inches), affordable and widely available even in remote locations. At several locations ($n = 5$), soil cores were collected
150 using a handheld motorized rotational Earth Auger (Stihl BT 121) with a 50 cm core barrel and 52 mm outside
151 diameter. Samples were split lengthwise into two halves: one half was analyzed to determine sediment characteristics,
152 volumetric ice content, and gravimetric water content. Disturbance material was removed from the core surface by
153 repeated scraping with a razor blade. The other half of each core was kept as a frozen archive to be used in the event
154 of laboratory error. Since the accurate determination of soil bulk density (BD) is crucial when calculating SOC, special
155 attention was paid to accurate soil volume estimation during field sampling. The target depth for soil cores was 100

156 cm, or until bedrock or massive ground ice (e.g. ice-wedges) was reached. Pedons were often extended beyond 100
157 cm depth (n = 313), in particular to assess full peat depth and organic/mineral transition in organic soils.

158 Wet or frozen samples were described and placed in double bags to assure no soil water was lost in transport. For each
159 sampled soil profile, pictures and notes were taken to describe land cover type, landform, elevation, slope and aspect,
160 surface moisture, and surface features. Specific observations regarding the collected sample depths, such as excess
161 ground ice (visual estimate, %), occurrence of large stones (visual estimate, %), colour (general description or using
162 a Munsell scale), soil structure, including signs of cryoturbation, roots and rooting depth were noted. Samples with
163 cryoturbated soil material were marked or rated on a scale from 1 to 3 according to the relative amount of cryoturbated
164 soil material. Soil texture, which refers to particle size and relative content of mineral components (sand, silt + clay)
165 is of importance as it affects the physical and chemical properties of a soil, including cryoturbation (Palmtag and
166 Kuhry, 2018). Soil texture was estimated for most samples using manipulation tests and assessment by hand in the
167 field under varying weather conditions. To avoid misinterpretation, we decided to combine silt and clay and refer to
168 them as one fine-grained soil texture class. In case of permafrost samples, subsamples were thawed, analyzed and
169 returned back to the sample bag. The land cover and vegetation community were described at all sites. For many sites,
170 vegetation cover was described in terms of relative plant functional type coverage per square meter. Beyond assigning
171 the profiles to land cover, vegetation data is not included in this database and not further discussed.

172



173

174 Figure 2: A three-dimensional field sampling protocol with typical soil layers in permafrost ground (reprinted from
175 Weiss 2017, p.12). The orange shapes represent the different sampling techniques for organic surface layer (block),
176 active layer sample from an excavated pit (fixed volume cylinder) and permafrost sampling (steel pipe).

177 2.3 Laboratory analysis

178 In the laboratory, soil samples ($n = 5315$) were weighed before and after oven-drying at $60-70^{\circ}\text{C}$ for at least 24 h (or
179 until no further weight change was observed) to determine field-moist mass (m_{ws}) and the oven-dried mass (m_d), thus
180 permitting the calculation of wet bulk density (BD_w) and dry bulk density (BD , g cm^{-3}) using the known sample
181 volume. To ensure that there was no remaining water in the organic rich and/or fine grained samples ($n=3684$),
182 subsamples of ~ 10 g were dried again at 105°C to verify the oven dried weights. After drying, samples were
183 homogenized and sieved to determine the concentration of coarse mineral fragments (CF, >2 mm, %). For a subset of
184 samples, particle size analysis was performed using a Malvern Mastersizer 3000 laser particle size analyzer (Malvern
185 Instruments Ltd, Malvern, UK), which can analyze particles in the range of $0.01-3500$ μm in diameter. It measures
186 the intensity of light scattered as a laser beam passes through a dispersed particulate sample. A detailed description of
187 these samples is given in Palmtag et al. (2018). Out of 5331 samples where OC % data is available, subsamples from
188 4471 samples were heated to 550°C for 5h to obtain organic matter content through loss on ignition (LOI; Heiri et
189 al., 2001), and about half of the samples ($n = 2960$), were heated to 950°C for 2 h to determine carbonate content (for
190 details, see Palmtag et al., 2015; 2016). To determine the elemental content of carbon and nitrogen (TOC and TN) and
191 their isotopic composition, 2674 samples were analysed using an Elemental Analyser (EA). If LOI950 following Heiri
192 et al. (2001) indicated presence of inorganic carbon $> 1\%$, samples were acid treated (Abisko, Sweden; Ny Ålesund,
193 Norway; Aktru, Altai mountains, Russia) with hydrochloric acid prior to determination of TOC. To estimate the
194 organic carbon % (OC %) for samples where only LOI was available (44 %), a polynomial regression model ($R^2 =$
195 95%) was performed between LOI550 and OC % from EA on samples for which both analyses were available at study
196 area level.

197 2.4 SOC/TN stock calculations and upscaling

198 Dry and wet bulk density (g cm^{-3}), sample volume (cm^3) and % carbon was used to calculate the volumetric contents
199 of water, organic soil material, mineral soil material and air for each sample. The soil organic carbon content (kg C
200 m^{-2}) was calculated for each sample separately based on dry bulk density (BD , g cm^{-3}), percentage organic C in the
201 sample (OC %), sample thickness T (cm), and coarse fraction correction (CF) (Equation 1). Equation 1 was also used
202 to calculate the TN content, in which OC % was replaced with N %.

$$203 \text{SOC}(\text{gC cm}^{-2}) = BD * OC \% * (1 - CF) * T \quad 1$$

204 SOC content for each pedon was calculated by summing up individual samples on 1 cm resolution until the maximum
205 sampling depth was reached. The pedons were assigned to a specific land cover class and the SOC content averaged

206 for different depth intervals (0–30 cm, 30–50 cm, 50–100 cm, 100–200 cm, 200–300 cm, and summed to 0–100 cm
207 and 0–300 cm). In areas with large stones in the soil column (e.g. alpine areas) or areas with massive ice bodies (e.g.
208 Yedoma deposits), it is also important to deduct the volume of stones or massive ice from the calculations. These
209 additional variables are not included in equation 1, but were accounted for in the SOC calculations at the pedon level.
210 If bedrock was encountered at any point, a SOC content of 0 kg C m⁻² was assigned for the remaining part down to
211 300 cm depth at that specific sampling site. In pedons where some increments were missing or the full sampling depth
212 was not reached, the nearest samples from the same pedon for BD and OC % were interpolated or extrapolated. To
213 avoid overestimation of the SOC storage, such extrapolations were only used where field notes showed that the
214 deposits were homogeneous and bedrock was not reached.

215 Masses of soil components (water (m_w , g), organic matter (m_{OM} , g) and mineral component (m_{min} , g)) were calculated
216 based on the laboratory analysis for all the individual samples. The mass of water was calculated as a difference
217 between field-moist mass and oven-dried mass. Organic matter mass was calculated from the OC % and dry sample
218 weight and multiplied by 2, which is a standard conversion factor between SOC and SOM (Pribyl, 2010). The mass
219 of the mineral fraction was calculated as a difference between dry sample mass and organic matter mass.

220 Volumetric fractions of soil components were calculated by dividing the volume of the component with the total
221 sample volume (V). We calculated component volumes from mass by assuming the following densities: 1 g cm⁻³ for
222 water, 0.91 g cm⁻³ for ice, 1.3 g cm⁻³ for organic matter (Farouki, 1981) and 2.65 g cm⁻³ mineral component. The
223 volumetric fraction of air was calculated as one minus the sum of the other fractions.

224 All profiles were assigned to land cover class based on field descriptions. Dry bulk density, SOC density, TN density
225 and the volumetric contents of mineral and organic matter and water and air were averaged according to land cover
226 classes for depths until 3 m using Python scripting language and pandas library (McKinney, 2011). Soil parameters
227 were assigned to pedon sample depth ranges and these were grouped according to land cover classes yielding means
228 and standard deviations for each centimetre of depth. Fractions of soil texture classes (sand and silt + clay) were
229 created using the same procedure by counting occurrences of texture classes within pedons. Typical soil stratigraphies
230 were generated for each class which can be used as input for permafrost modelling and mapping (e.g. Westermann et
231 al., 2013; 2017; Czekirda et al., 2019).

232 For the upscaling, we used the land cover map from the Global ESA Land cover Climate Change Initiative (CCI)
233 project at 300 m spatial resolution (<http://maps.elie.ucl.ac.be/CCI/viewer/index.php>). The overall classification
234 accuracy, based on 3167 random sampling cases, is stated as 73 % (Defourny et al., 2008). The land cover class dataset
235 for upscaling was generated from ESA CCI land cover yearly products from period 2006 to 2015 (corresponding to
236 the sampling period) by identifying prevailing land cover classes within this period. The extent of the Yedoma land
237 cover classes was defined from shapefiles of the Yedoma database by Strauss et al., (2017), where all the layers were
238 used except for QG2500k, which is showing the lowest probability of Yedoma occurrence.

239 Since the ESA land cover product uses a different nomenclature for land cover types with different sub-categories,
240 similar classes were amalgamated to fit our tiered land cover system (Table 2). Several minor classes consisting of

241 single pixels spread over the map were generalized and merged with the class surrounding the pixel. We defined Tier
 242 II Yedoma classes (Yedoma tundra and Yedoma forest) according to the ESA CCI Land cover classes coinciding with
 243 Yedoma deposits (Table 3).

244 The spatial land cover extent was constrained to the Northern Hemisphere permafrost region indicating probability of
 245 permafrost occurrence but not the actual area underlain by permafrost (Obu, 2021). This dataset stretches over
 246 17.9×10^6 km² of the Northern Hemisphere, and is based on equilibrium state model for the temperature at the top of
 247 the permafrost (TTOP) for the 2000–2016 period (Obu et al., 2019).

248 Table 3: Amalgamation of ESA’s CCI land cover classes with the Tier class system above the Yedoma deposits.

CCI class	ESA CCI landcover	TIER I class	TIER II class
40	Mosaic natural vegetation (tree, shrub, herbaceous cover) (>50 %)	1	1.1 & 5.2
50	Tree cover, broadleaved, evergreen, closed to open (>15 %)	1	1.1 & 5.2
60	Tree cover, broadleaved, deciduous, closed to open (>15 %)	1	1.1 & 5.2
61	Tree cover, broadleaved, deciduous, closed (>40 %)	1	1.1 & 5.2
70	Tree cover, needleleaved, evergreen, closed to open (>15 %)	1	1.2 & 5.2
71	Tree cover, needleleaved, evergreen, closed (>40 %)	1	1.2 & 5.2
72	Tree cover, needleleaved, evergreen, open (15-40 %)	1	1.2 & 5.2
80	Tree cover, needleleaved, deciduous, closed to open (>15 %)	1	1.3 & 5.2
90	Tree cover, mixed leaf type (broadleaved and needleleaved)	1	1.1 & 5.2
100	Mosaic tree and shrub (>50 %) / herbaceous cover (<50 %)	1	1.1 & 5.2
110	Mosaic herbaceous cover (>50 %) / tree and shrub (<50 %)	1	1.3 & 5.2
120	Shrubland	2	2.1 & 5.1
121	Evergreen shrubland	2	2.1 & 5.1
122	Deciduous shrubland	2	2.1 & 5.1
130	Grassland	2	2.2 & 5.1
140	Lichens and mosses	2	2.2 & 5.1
150	Sparse vegetation (tree, shrub, herbaceous cover) (<15 %)	2	2.1 & 5.1
152	Sparse shrub (<15 %)	2	2.1 & 5.1
160	Tree cover, flooded, fresh or brackish water	3	3.1
180	Shrub or herbaceous cover, flooded, fresh/saline/brackish water	3	3.1
200	Bare areas	5	4.1
201	Consolidated bare areas	5	4.1
202	Unconsolidated bare areas	5	4.1

249
 250 The upscaling to estimate the total carbon storage in the northern circumpolar permafrost region was performed in
 251 ArcGIS Pro (ESRI, Redlands, CA, USA) by multiplying the mean SOC storage for each Tier I and Tier II class with
 252 the spatial extent of the corresponding CCI land cover class. To determine reasonable error estimates for carbon stocks
 253 within the permafrost region, we used a spatially weighed 95 % confidence interval (CI) as described by Thompson
 254 (1992) assuming that our residuals are normally distributed (Hugelius, 2012).

255
$$CI = t * \sqrt{\sum((a_i^2 * SD_i^2)/n_i)}$$
 2

256 The CI accounts for the relative spatial extent, carbon stock variations in pedons and number of replicates in each
 257 upscaling class. Replicates were only considered for pedons reaching the full sampling depth, resulting in fewer
 258 replicates available with increasing sampling depth. In equation 2: t is the upper $\alpha/2$ of a normal distribution ($t \approx 1.96$),
 259 a the % of the area; SD is the standard deviation, n is to the number of replicates and i refers the specific Tier class.

260 **3. Results**

261 **3.1 SOC estimates**

262 Using our pedon based dataset, we obtain SOC stock estimates within the northern circumpolar permafrost region of
 263 379.7 and 812.6 Pg for 0–100 cm and 0–300 cm depth, respectively. Table 4 shows mean SOC storage (kg C m^{-2}) and
 264 total SOC stock for all depth increments, including 95 % confidence intervals. The upscaling using this new pedon
 265 data shows that almost half of SOC in the northern circumpolar permafrost region is stored in the top meter. The three
 266 most abundant classes together (deciduous needleleaf forest, shrub tundra and graminoid / forb tundra) occupy 67 %
 267 of the permafrost region (Table 5) and store most of terrestrial SOC in the northern circumpolar region (74 %). The
 268 permafrost wetland class has the largest SOC content to 300 cm with 112.2 kg C m^{-2} , but has only a small areal
 269 coverage in the ESA LCC product (1.4 %) which results in a total SOC storage contribution of 3.5 % within the
 270 permafrost region. Figure 3 illustrates the spatial distribution of total SOC storage (kg C m^{-2}) to a depth of 0–100 cm
 271 and 0–300 cm for the circumpolar permafrost region. Spatially, the SOC distribution in Figure 3 is following the same
 272 pattern and highlights the largest SOC content predominantly in permafrost peatlands in Western Siberia, Russia and
 273 the Nunavut territory in Canada. Despite that, more than 77% of the area has a SOC storage to a depth of 300 cm
 274 higher than 50 kg m^{-2} .

275 Table 4: Landscape mean and total SOC storage with 95 % CI for the different depth increments for the northern
 276 circumpolar permafrost region, excluding water bodies and permanent snow and ice.

Depth increment	n:	Mean SOC storage (kg C m^{-2})	95 % CI ^a		Total SOC in Pg	95 % CI ^a
0–30 cm	452	9.0	±	1.4	160.0	± 25
30–50 cm	402	3.9	±	0.5	69.2	± 8
50–100 cm	328	8.4	±	1.4	150.5	± 25
100–200 cm	257	12.4	±	1.9	222.0	± 35
200–300 cm	253	11.8	±	1.7	211.0	± 31
0–100 cm	328	21.3	±	3.2	379.7	± 58
0–300 cm	253	45.5	±	7.6	812.6	± 136

277

278 ^a The 95 % confidence interval refers to landscape mean SOC storage and total SOC storage

279 Table 5: Mean and total SOC storage for (A) 0–100 cm and (B) 0–300 cm soil depth separated for the different Tier
 280 classes in the northern circumpolar permafrost region, excluding water bodies and permanent snow and ice.

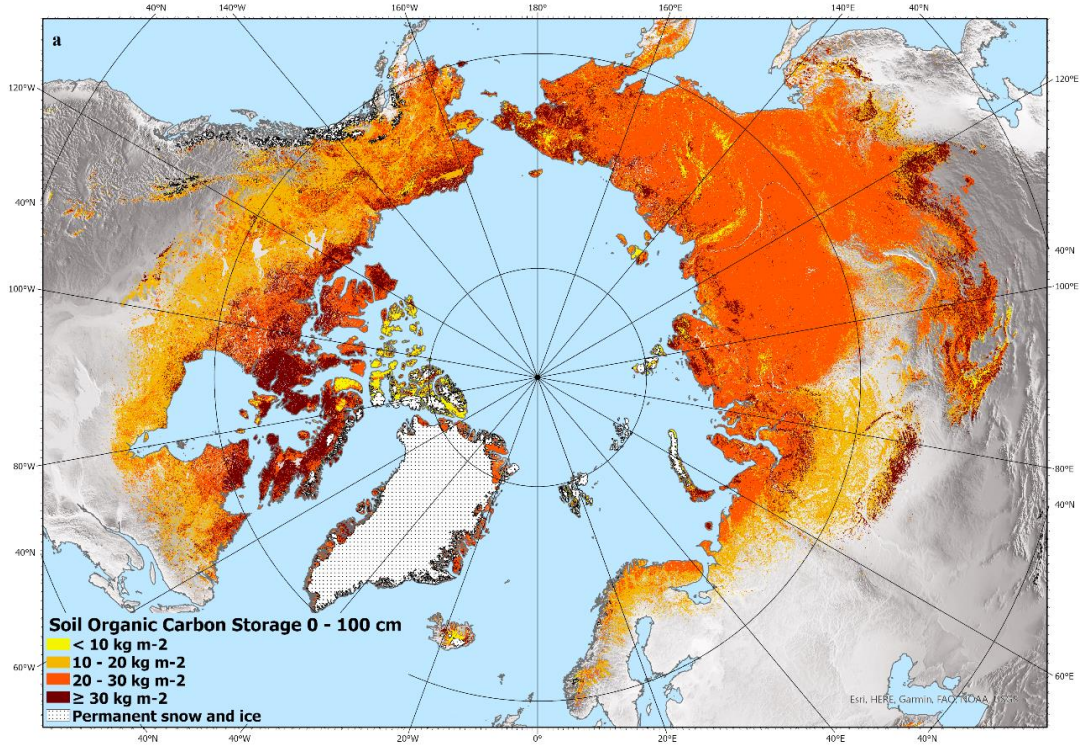
A	Tier class	LCC class	n ^a :	Area (million km ²)	Area %	Mean	SD ^b	Total SOC in Pg	Total SOC storage %
						SOC storage (kg C m ⁻²) _b			
1.1	Deciduous forest	broadleaf	5	0.85	4.8 %	16.5	9.3	14.1	3.7
1.2	Evergreen forest	needleleaf	4	2.54	14.3 %	14.6	12.8	37.1	9.8
1.3	Deciduous forest	needleleaf	28	5.20	29.1 %	20.5	20.3	106.5	28.1
2.1	Shrub tundra		54	3.97	22.3 %	22.3	21.7	88.5	23.3
2.2	Graminoid / forb tundra		118	2.85	15.9 %	31.6	23.0	90.0	23.7
3.1	Permafrost wetlands		61	0.25	1.4 %	37.8	37.8	9.6	2.5
3.2	Non-permafrost wetlands		10	0.76	4.3 %	17.8	14.7	13.5	3.6
5.1	Barren		39	0.85	4.8 %	9.4	12.0	8.0	2.1
7.1	Yedoma tundra		8	0.27	1.5 %	28.1	17.0	7.7	2.0
7.2	Yedoma forest		1	0.30	1.7 %	16.1	0.0	4.8	1.3

B	Tier class	LCC class	n ^a :	Area (million km ²)	Area %	Mean	SD ^b	Total SOC in Pg	Total SOC storage %
						SOC storage (kg C m ⁻²) _b			
1.1	Deciduous forest	broadleaf	2	0.85	4.8 %	33.2	22.8	28.3	3.5
1.2	Evergreen forest	needleleaf	2	2.54	14.3 %	23.0	16.3	58.7	7.2
1.3	Deciduous forest	needleleaf	14	5.20	29.1 %	38.3	33.3	199.2	24.5
2.1	Shrub tundra		50	3.97	22.3 %	49.2	50.8	195.6	24.1
2.2	Graminoid / forb tundra		114	2.85	15.9 %	72.2	67.5	205.4	25.3
3.1	Permafrost wetlands		49	0.25	1.4 %	112.2	121.5	28.4	3.5
3.2	Non-permafrost wetlands		7	0.76	4.3 %	74.5	70.5	56.6	7.0
5.1	Barren		9	0.85	4.8 %	11.7	14.9	10.0	1.2
7.1	Yedoma tundra		5	0.27	1.5 %	64.1	37.7	17.5	2.2
7.2	Yedoma forest		1	0.30	1.7 %	43.0	0.0	13.0	1.6

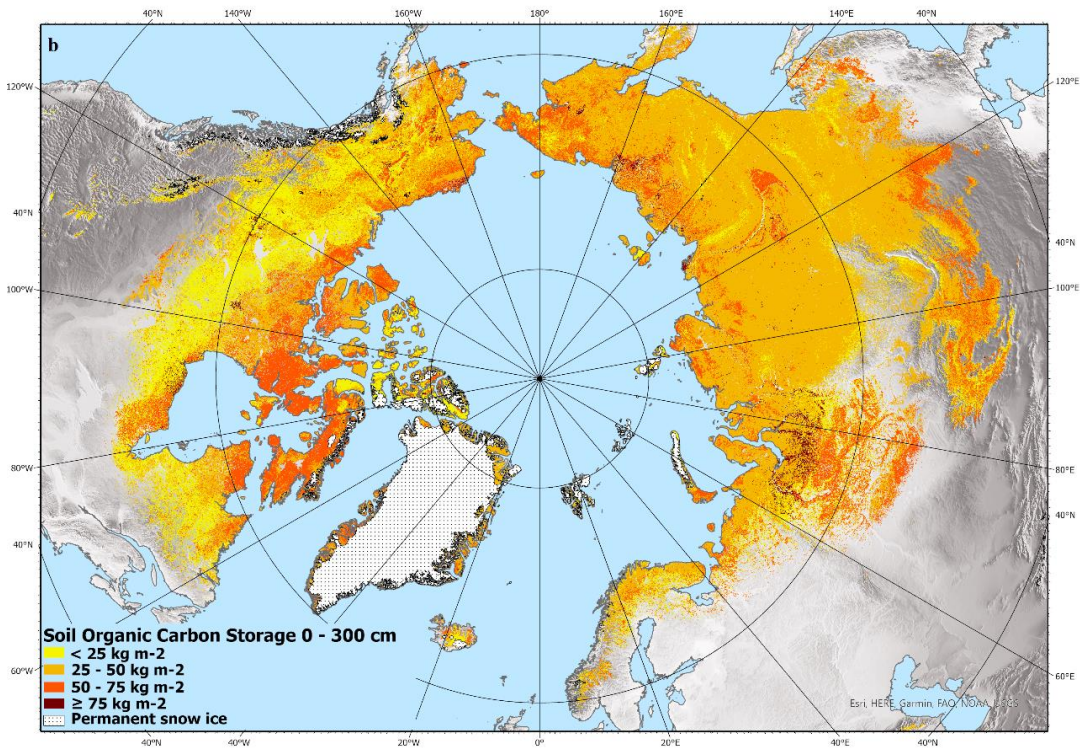
281

282 ^a The number of sampled pedons reaching a full depth of 100 cm or 300 cm, respectively.

283 ^b Mean SOC storage and SD calculations includes pedons which are not reaching the full section depth.



284



285

286 Figure 3. Estimated total SOC storage (kg C m^{-2}) to a depth of 0–100 cm (a) and 0–300 cm (b) in northern circumpolar
 287 permafrost region. North Pole Lambert azimuthal equal area projection (datum: WGS 84). Base map: Made with
 288 Natural Earth.

289 **3.2 TN estimates**

290 Our estimates show that the TN stocks down to 100 cm and 300 cm depth in the northern circumpolar permafrost
 291 region are 21.1 Pg and 55.0 Pg, respectively. Table 6 presents the mean and total TN storage for different depth
 292 increments with their 95% confidence interval. As with SOC storage, the most abundant land cover classes (deciduous
 293 needleleaf forest, shrub tundra and graminoid / forb tundra) store most (68 %) of the total TN in the permafrost region.
 294 The land cover classes permafrost and non-permafrost wetlands have the largest TN storage with a mean of up to 7
 295 kg N m⁻² for the 0–300 cm soil depth (Table 7). Figure 4 illustrates the spatial distribution of total TN storage (kg N
 296 m⁻²) for the circumpolar permafrost region for two depth intervals, 0–100 cm and 0–300 cm. The spatial distribution
 297 of TN has a similar pattern to SOC and is highlighting the permafrost peatlands in Western Siberia, Russia and the
 298 Nunavut territory in Canada.

299 Table 6: Mean and total TN storage with 95 % CI for the different depth increments for the northern circumpolar
 300 permafrost region, excluding water bodies and permanent snow and ice.

Depth increment		Mean TN storage (kg N m⁻²)		95 % CI^a	Total TN in Pg		95 % CI^a
0–30 cm	271	0.5	±	0.1	8.1	±	1.5
30–50 cm	250	0.2	±	0.0	4.2	±	0.5
50–100 cm	208	0.5	±	0.1	8.8	±	1.1
100–200 cm	175	1.0	±	0.2	17.1	±	2.8
200–300 cm	169	0.9	±	0.2	16.8	±	3.7
0–100 cm	208	1.2	±	0.3	21.1	±	4.7
0–300 cm	169	3.1	±	0.8	55.0	±	15.1

301

302 ^a The 95 % confidence interval refers to landscape mean TN storage and total TN storage

303 Table 7: Mean and total TN storage for (A) 0–100 cm and (B) 0–300 cm soil depth separated for the different Tier
 304 classes within the northern circumpolar permafrost region, excluding water bodies and permanent snow and ice.

A	Tier class	LCC class	n ^a :	Area (million km ²)	Area %	Mean TN storage		Total TN in Pg	Total TN storage %
						(kg N m ⁻²) ^b	SD ^b		
1.1	Deciduous forest	broadleaf	2	0.85	4.8 %	1.0	0.6	0.9	4.1
1.2	Evergreen forest	needleleaf	1	2.54	14.3 %	0.8	0.8	1.9	9.2
1.3	Deciduous forest	needleleaf	19	5.20	29.1 %	1.0	0.6	5.1	24.3
2.1	Shrub tundra		32	3.97	22.3 %	1.6	1.5	6.4	30.3
2.2	Graminoid / forbtundra		72	2.85	15.9 %	1.5	0.9	4.3	20.3
3.1	Permafrost wetlands		46	0.25	1.4 %	2.4	2.5	0.6	2.8
3.2	Non-permafrost wetlands		4	0.76	4.3 %	0.7	0.6	0.5	2.4
5.1	Barren		26	0.85	4.8 %	0.7	0.9	0.6	2.6
7.1	Yedoma tundra		5	0.27	1.5 %	1.6	0.6	0.4	2.0
7.2	Yedoma forest		1	0.30	1.7 %	1.4	0.0	0.4	2.0

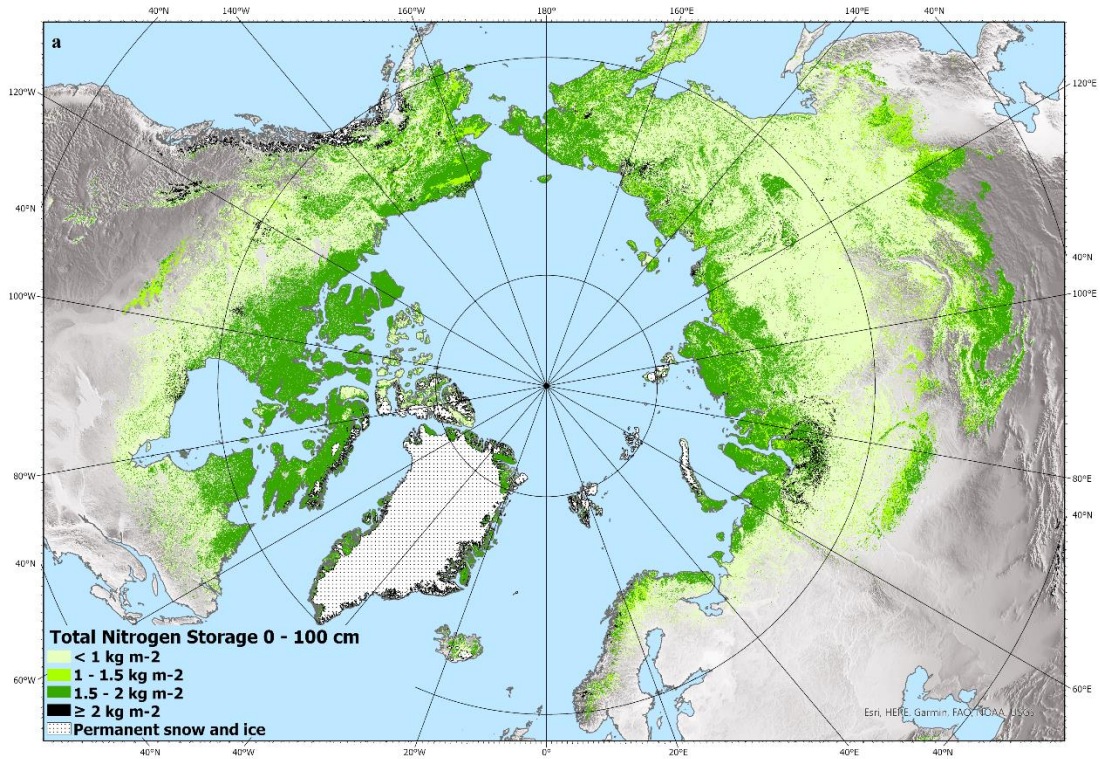
B	Tier class	LCC class	n ^a :	Area (million km ²)	Area %	Mean TN storage		Total TN in Pg	Total TN storage %
						(kg N m ⁻²) ^b	SD ^b		
1.1	Deciduous forest	broadleaf	2	0.85	4.8 %	2.8	1.7	2.4	4.3
1.2	Evergreen forest	needleleaf	1	2.54	14.3 %	1.9	2.3	4.8	8.8
1.3	Deciduous forest	needleleaf	12	5.20	29.1 %	2.4	1.3	12.6	23.0
2.1	Shrub tundra		30	3.97	22.3 %	3.9	3.4	15.5	28.2
2.2	Graminoid / forbtundra		69	2.85	15.9 %	3.4	2.2	9.6	17.5
3.1	Permafrost wetlands		40	0.25	1.4 %	7.0	7.8	1.8	3.2
3.2	Non-permafrost wetlands		2	0.76	4.3 %	6.4	6.6	4.9	8.9
5.1	Barren		9	0.85	4.8 %	0.8	1.1	0.7	1.2
7.1	Yedoma tundra		3	0.27	1.5 %	5.6	2.2	1.5	2.8
7.2	Yedoma forest		1	0.30	1.7 %	4.1	0.0	1.2	2.2

305

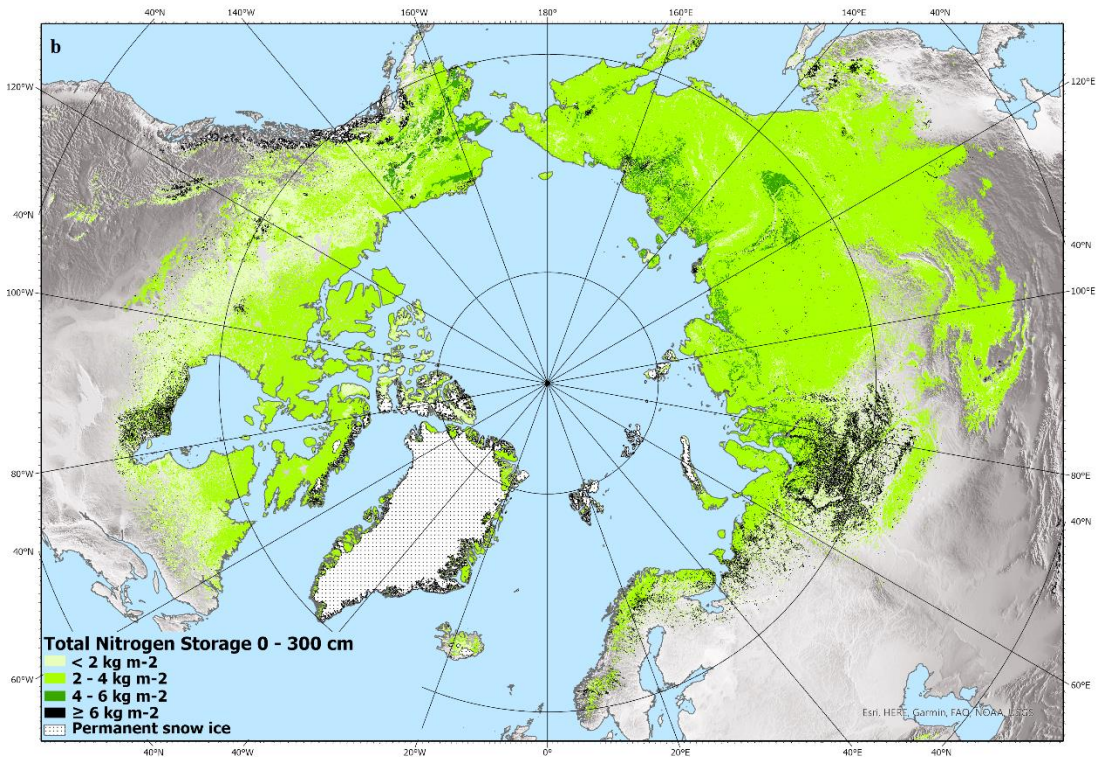
306 ^a The number of sampled pedons reaching a full depth of 100 cm or 300 cm, respectively.

307 ^b Mean TN storage and SD calculations includes pedons which are not reaching the full section depth.

308



309



310

311 Figure 4. Estimated total Nitrogen storage (kg N m^{-2}) to a depth of 0–100 cm and 0–300 cm in northern circumpolar
 312 permafrost region. North Pole Lambert azimuthal equal area projection (datum: WGS 84). Base map: Made with
 313 Natural Earth.

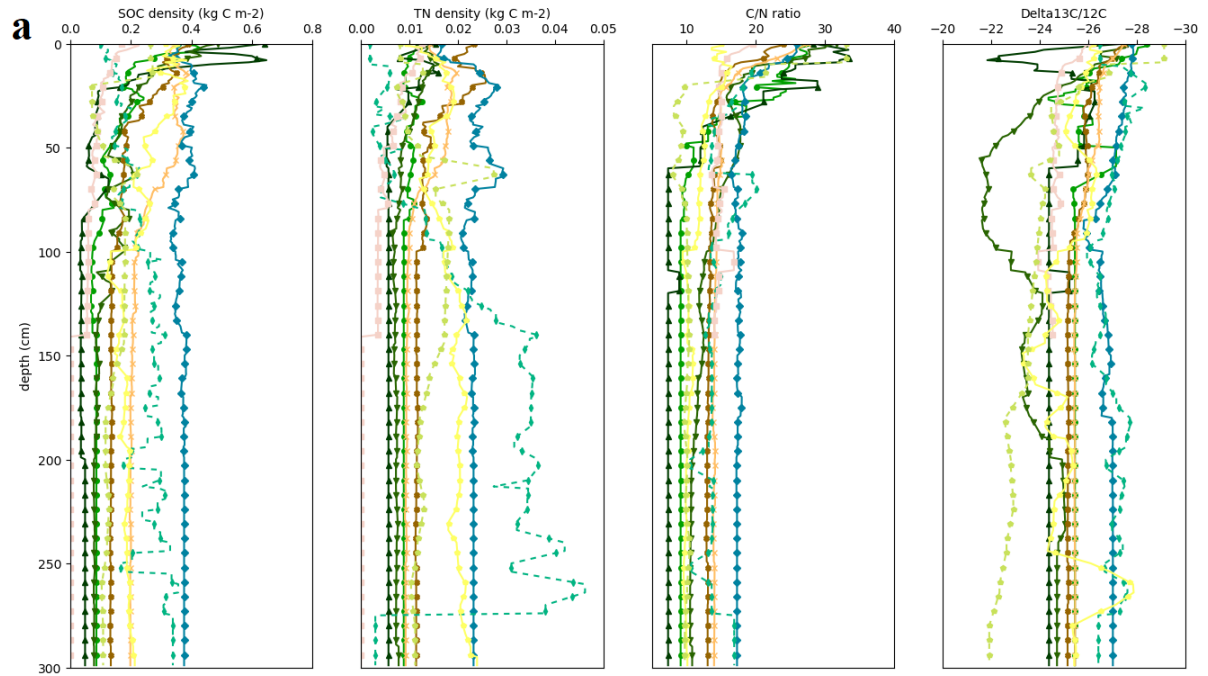
314 **3.3 C/N ratio and $\delta^{13}\text{C}$**

315 Carbon to nitrogen ratios are often used as an indicator for SOM decomposition. As during the metabolic activity by
316 microorganisms more carbon than nitrogen is released, the C/N ratio decreases with a higher degree of humification.
317 This is why C/N ratios usually decrease with depth, as deeper layers are typically older and more decomposed (Kuhry
318 and Vitt, 1996). Our data confirms this pattern of fast decreasing C/N ratio with depth in all land cover classes to about
319 50 cm of depth followed by weak decline throughout the full pedon depth (Figure 5 a). The C/N values of SOC rich
320 top soil organic and peat samples are significantly higher than from the mineral samples ($p < 0.05$). The C/N ratios
321 together with stable carbon isotopes ($\delta^{13}\text{C}$) can be used to gain insight into the biochemical processes of SOM,
322 botanical origin with depth and the degradation state (Kracht and Gleixner, 2000). The lowest $\delta^{13}\text{C}$ values,
323 predominantly in the upper 50 cm, indicates that this SOM is more easily available for microbial utilization with
324 lowest values in peatlands connected to differences in hydrology.

325

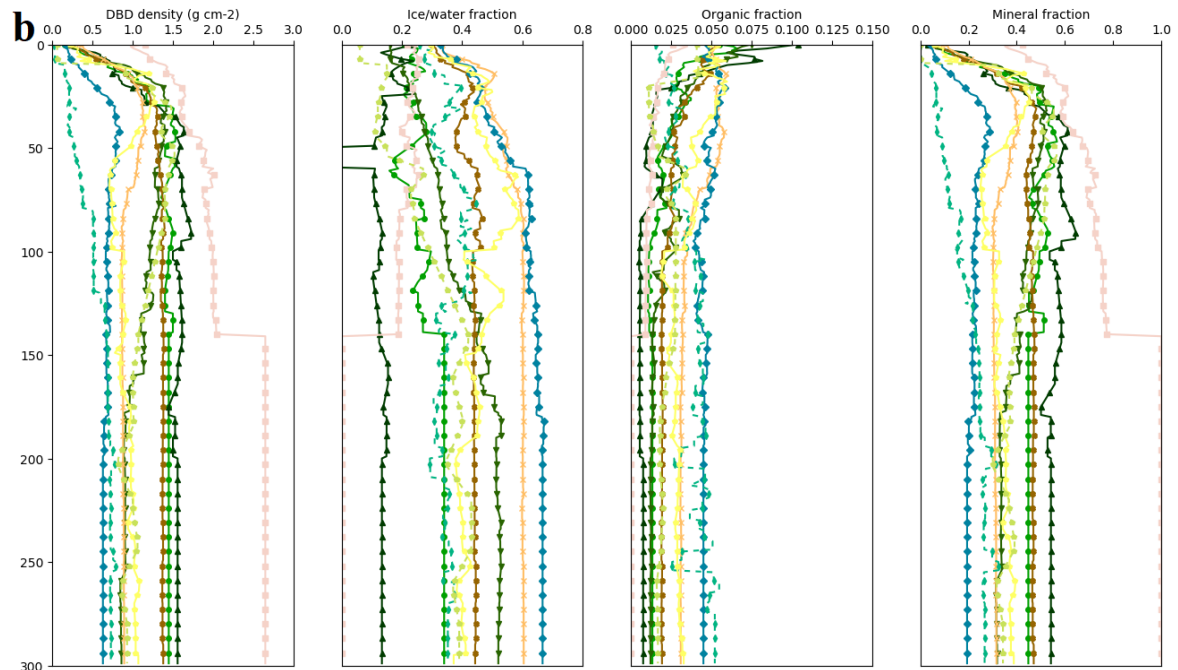
326 **3.4 Soil stratigraphies**

327 Figure 5 illustrates averaged vertical soil stratigraphies for SOC and TN density, C/N ratio with $\delta^{13}\text{C}$, dry bulk density,
328 volumetric fractions for water/ice, organic, mineral, air and texture (sand, silt + clay fraction) separated by land cover
329 class to 300 cm depth. The data shows clear differences occurring in the more variable top meter in comparison to the
330 rather stable second and third meter with the exception in non-permafrost wetlands where the TN and SOC density is
331 more variable below 100 cm depth, which results from only 2 stratigraphically different available pedons where TN
332 data is available (Table 7). The permafrost wetland class shows the highest and consistent stratigraphy for SOC and
333 TN density, which is due to the high organic fraction of these soils. In comparison, the barren has the lowest SOC and
334 TN, as these soils are dominated by the coarse mineral fraction and from ca. 140 cm depth even our deepest barren
335 sample reached bedrock. While the stratigraphy for the Yedoma classes proves the Yedoma typical ice-rich silt
336 sediments noticeable in the high silt + clay and high water/ice fraction. Stratigraphy for DBD shows a strong
337 dependence with the mineral fraction and almost identical soil stratigraphy.

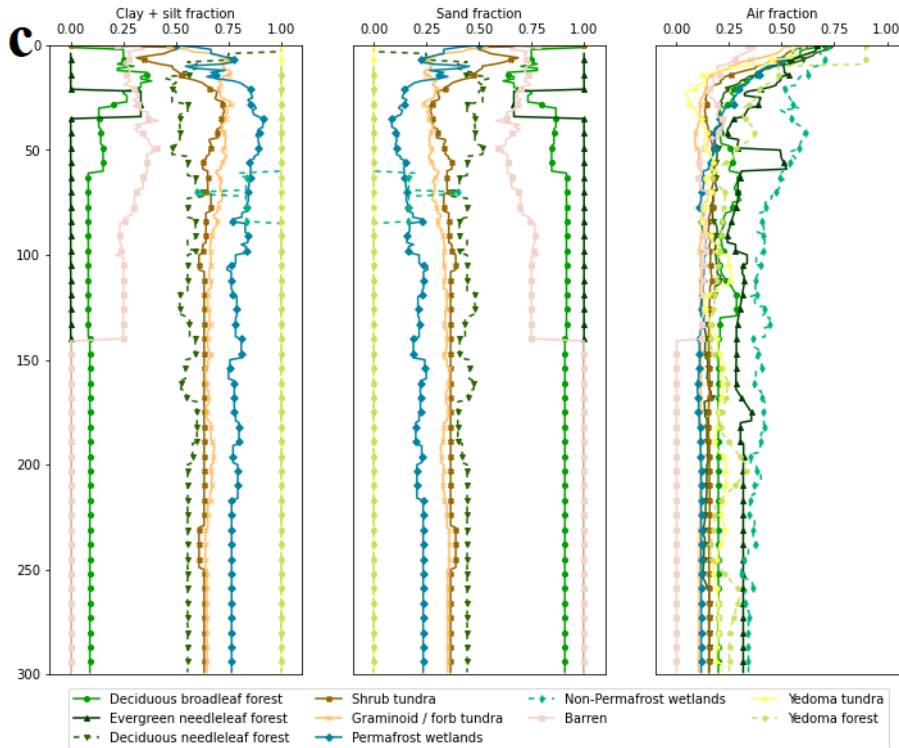


338

339



340



341
 342 Figure 5. Typical vertical soil stratigraphies for all the land cover classes to 300 cm depth separated for SOC density,
 343 TN density, C/N ratio and Delta 13C/12C (a); DBD density, Ice/water fraction, Organic fraction and Mineral fraction
 344 (b); Clay + silt fraction, Sand fraction and Air fraction (c).

345 **4. Discussion**

346 The goal of the field studies to collect this dataset has mainly been to improve the knowledge base for studies of
 347 climate feedbacks resulting from permafrost thaw. This new open access database provides georeferenced and quality
 348 assessed soil profile data to serve different scientific communities. While there are multiple databases available
 349 containing data on soil carbon storage (Hugelius et al., 2013, Michaelson et al., 2013, Mishra et al., 2021), there is
 350 still a lack of soil field data covering a wider range of properties within the hard-accessible northern circumpolar
 351 permafrost region.

352 To test and exemplify usage of the soil profile database, we used our field-based metadata to classify soil profiles
 353 according to a coherent land cover scheme and combined it with ESA's land cover product to provide a new estimate
 354 of soil organic carbon storage in the northern circumpolar permafrost region. Our estimate for SOC is 380 Pg \pm 58 Pg
 355 to 100 cm soil depth and 813 Pg \pm 136 Pg to 300 cm soil depth for the permafrost region occupying an area of
 356 17.9×10^6 km² (excluding area of Tibetan permafrost region, permanent snow and ice and water bodies). In
 357 comparison, Hugelius et al., (2014) estimated SOC stocks in the northern circumpolar permafrost region (17.8×10^6
 358 km² excluding exposed bedrock, glaciers and ice-sheets and water bodies) to be 472 \pm 27 Pg and 1035 \pm 150 Pg to
 359 100 cm and 300 cm for soils, respectively. A recent publication by Mishra et al., (2021) based on > 2700 soil profiles

360 with environmental variables in a geostatistical mapping framework, estimated a total SOC stock of 510 Pg (– 78 to
361 +79 Pg) and 1000 (– 170 to +186 Pg) to 100 cm and 300 cm, respectively. Although our values are a bit lower than
362 their estimates, they are within each other ranges. Usage of a different landcover based upscaling approach could be
363 the cause of some of these differences.

364 Despite the importance of nitrogen for microbial decomposition and plant productivity processes, few large-scale
365 datasets are available on TN storage. Our TN estimate for the northern circumpolar permafrost region is 21 Pg \pm 5 Pg
366 to 100 cm soil depth and 55 Pg \pm 15 Pg to 300 cm soil depth. This is in line with the only other circumpolar estimate
367 of 66 Pg (\pm 35 Pg) by Harden et al. (2012).

368 According to Kuhry and Vitt (1996), C/N ratios of peat deposits decrease over time due to cumulative anaerobic
369 degradation whereas aerobic decomposition and release of CO₂ is lowering the C/N ratios in organic and mineral soil
370 horizons (Ping et al., 1998). Our data show that the C/N ratios in organic soil horizons and peat layers were
371 significantly higher than from mineral subsoil horizons. Based on this, we can use the C/N ratio data to assess the
372 relative degree of SOM decomposition on circumpolar scale. However, C/N ratios and stable carbon isotopes are also
373 affected by the original plant type and the climate which can in addition contribute to changes over time.

374 A key element to this upscaling exercise is the accuracy of the land cover dataset. Despite the relatively high spatial
375 resolution of 300 m, many Arctic landscape features cannot be represented at this scale. Although, ESA's land cover
376 map has a good overall accuracy of 73 %; however, this means that 27 % of the land cover is possibly mismatched
377 and in need of improvement. Moreover, the accuracy for natural and semi-natural aquatic vegetation, which
378 corresponds to our wetland class, is unfortunately as low as 19 % which corresponds to our class (wetland). According
379 to Hugelius et al. (2020), the areal extent of peatlands for the northern permafrost region (3.7×10^6 km²) is almost
380 four times the ESA's land cover product estimated areal extent (1.0×10^6 km²). Therefore, wrongly classified areas
381 would partly explain our lower estimate for SOC and TN on a circumpolar scale since the wetland classes have the
382 largest SOC and TN contents, particularly at greater depths (100–300 cm). This is evident on maps (Figure 3 and
383 Figure 4) where areas classified as peatlands are clearly standing out with their high SOC and TN contents. If we
384 exchange the ESA wetland areal coverage for the values from Hugelius et al. (2020) to 3.7×10^6 km² (2.0×10^6 km²
385 in permafrost-free peatlands and 1.7×10^6 km² permafrost-affected peatlands) and deduct this in proportion from the
386 other classes, our updated SOC and TN stock to 300 cm soil depth increases from 813 Pg \pm 136 Pg to 954 Pg \pm 162
387 Pg and from 55 Pg \pm 15 Pg to 66 Pg \pm 22 Pg, respectively.

388 Even though the current estimates are based on 651 soil pedons from 16 different study areas, there are uncertainties
389 and data gaps for several regions and ecosystems. With e.g. only one high alpine site and one Yedoma forest site,
390 several areas are highly underrepresented. Also, the study areas are concentrated in European and Russian locations
391 which additionally increases the uncertainties in current estimates. Therefore, combining this data with other datasets
392 especially from North America, Tibet, Yedoma sites and a different wetland extent would substantially reduce
393 potential error sources and create a more complete picture of SOC and TN storage estimates from land cover based
394 upscaling. To our knowledge, this is the first product which presents a more complete dataset in regard to variables
395 on a circumpolar scale that are commonly used to parameterize earth system models. With this database we aim to

396 provide georeferenced point data that can easily be implemented and used for geospatial analysis at a circumpolar
397 scale. This upscaling approach was chosen because this database can be easily extended with additional sampling
398 sites, higher-resolution land cover maps that will further increase the resolution on a circumpolar scale. This data can
399 also be used for upscaling in a particular area of interest. This will assist to quantify and model ongoing pedological
400 and ecological processes relevant to climate change. Furthermore, this may help identifying regions that are more
401 vulnerable to permafrost degradation and greenhouse gas release due to knowledge on texture, water/ice content or
402 SOC storage.

403 **5. Conclusion**

404 This dataset represents a substantial contribution of high-quality soil pedon data and metadata across the northern
405 permafrost region. Our land cover based estimates of total SOC to 100 cm and 300 cm soil depth are $380 \text{ Pg} \pm 58 \text{ Pg}$
406 and $813 \text{ Pg} \pm 136 \text{ Pg}$, respectively. In addition, we contribute with novel TN estimates for the different land cover
407 classes and depth increments. Our TN estimate to 100 cm and 300 cm soil depth are $21.1 \pm 4.7 \text{ Pg}$ and $55 \text{ Pg} \pm 15 \text{ Pg}$
408 which is in line with the only other product available on that scale for TN. Despite a different methodology, are similar
409 but on the lower edge to other recent numbers. We provide data for a wide range of environments and geographical
410 regions across the permafrost region including georeferencing and metadata. This serves as a base that can be easily
411 combined and extended with data from other sources, as several regions are underrepresented (Alaska, Canada, Tibet).
412 This dataset offers high scientific value as it also contains data on chemical and physical soil properties across the
413 northern circumpolar permafrost region. This additional data can be used to develop or parametrize broad scale models
414 and to help better understand different aspects of the permafrost-carbon climate feedback.

415 **6. Data access**

416 Two separated datasets are freely available on the Bolin Centre data set repository (<https://bolin.su.se/data/>). The
417 dataset (Detailed pedon data on soil carbon and nitrogen for the northern permafrost region,
418 <https://doi.org/10.17043/palmtag-2022-pedon-1>) (Palmtag et al., 2022a) is a geospatial dataset of physical and
419 chemical soil properties from 651 soil pedons and the second dataset (A high spatial resolution soil carbon and nitrogen
420 dataset for the northern permafrost region, <https://doi.org/10.17043/palmtag-2022-spatial-1>) (Palmtag et al., 2022b)
421 contains GIS grids of the northern circumpolar permafrost region for SOC, TN and C/N ratios for the different depth
422 increments.

423

424 **Funding**

425 This study was funded through the European Space Agency CCI + Permafrost project (4000123681/18/I-NB), the
426 European Union Horizon 2020 research and innovation project Nunataryuk (773421), the Changing Arctic Ocean
427 (CAO) program project CACOON (NE/R012806/1) and the Swedish Research Council (2018-04516).

428

429 **Author contribution**

430 GH, PK, SW and JP designed the concept of the study. JO wrote the script in Python. JP wrote the initial draft of the
431 manuscript. All authors contributed to the writing and editing of the manuscript.

432 **Competing Interests**

433 The authors declare that they have no conflict of interest.

434 **Acknowledgements**

435 We thank the ESA CCI Land Cover project for providing the data, which was used for upscaling our product to
436 circumpolar scale.

437 **References**

438 Batjes, N.H.: Harmonized soil property values for broad-scale modelling (WISE30sec) with estimates of global soil
439 carbon stocks, *Geoderma*, Vol. 269, <https://doi.org/10.1016/j.geoderma.2016.01.034>, 2016.

440 Biskaborn, B. K., Smith, S. L., Noetzli, J., Matthes, H., Vieira, G., Streletskiy, D. A., Schoeneich, P., Romanovsky,
441 V. E., Lewkowicz, A. G., Abramov, A., Allard, M., Boike, J., Cable, W. L., Christiansen, H. H., Delaloye, R.,
442 Diekmann, B., Drozdov, D., Etzelmüller, B., Grosse, G., Guglielmin, M., Thomas Ingeman-Nielsen, T., Ketil Isaksen,
443 K., Ishikawa, M., Johansson, M., Johannsson, H., Joo, A., Kaverin, D., Kholodov, A., Konstantinov, P., Kröger, T.,
444 Lambiel, C., Lanckman, J.-P., Luo, D., Malkova, G., Meiklejohn, I., Moskalenko, N., Oliva, M., Phillips, M., Ramos,
445 M., Sannel, A. B. K., Sergeev, D., Seybold, C., Skryabin, P., Vasiliev, A., Wu, Q., Yoshikawa, K., Zheleznyak, M.
446 and Lantuit, H.: Permafrost is warming at a global scale, *Nature Communications*, 10(1), 264,
447 <https://doi.org/10.1038/s41467-018-08240-4>, 2019.

448 Czekirda, J., Westermann, S., Etzelmüller, B. and Johanneson, T.: Transient modelling of permafrost distribution in
449 Iceland. *Frontiers in Earth Science*, 7, 130, <https://doi.org/10.3389/feart.2019.00130>, 2019.

450 Defourny, P., Schouten, L., Bartalev, S.A., Bontemps, S., Caccetta, P., de Wit, A.J.W., Di Bella, C., Gerard, B., Giri,
451 C., Gong, V., Hazeu, G.W., Heinemann, A., Herold, M., Knoops, J., Jaffrain, G., Latifovic, R., Lin, H., Mayaux, P.,
452 Mâcher, C.A., Nonguierma, A., Stibig, H.J., Van Bogaert, E., Vancutsem, C., Bicheron, P., Leroy, M. and Arino, O.:
453 Accuracy assessment of a 300 m global land cover map: The GlobCover experience. Available online: [http://www.un-](http://www.un-spider.org/space-application/space-application-matrix/accuracy-assessment-300-m-global-land-cover-map-globcover)
454 [spider.org/space-application/space-application-matrix/accuracy-assessment-300-m-global-land-cover-map-](http://www.un-spider.org/space-application/space-application-matrix/accuracy-assessment-300-m-global-land-cover-map-globcover)
455 [globcover](http://www.un-spider.org/space-application/space-application-matrix/accuracy-assessment-300-m-global-land-cover-map-globcover) (accessed on 07 January 2022), 2008.

456 ESA Climate Change Initiative-Landcover visualization interface, Available from:
457 <http://maps.elie.ucl.ac.be/CCI/viewer/index.php> (accessed on 07 January 2022), 2017.

458 Farouki, O. T.: Thermal Properties of Soils, Cold regions research and engineering lab Hanover NH [online] Available
459 from: <https://apps.dtic.mil/docs/citations/ADA111734> (accessed on 07 January 2022), 1981.

460 Flato, G. M.: Earth system models: an overview, 2, 783–800, <https://doi.org/10.1002/wcc.148>, 2011.

461 Fritz, M., Vonk, J.E. and Lantuit, H.: Collapsing Arctic coastlines, *Nature Climate Change*, volume 7,
462 <https://doi.org/10.1038/nclimate3188>, 2017.

463 Fuchs, M., Kuhry, P., and Hugelius, G.: Low below-ground organic carbon storage in a subarctic Alpine permafrost
464 environment, *The Cryosphere*, 9, 427–438, <https://doi.org/10.5194/tc-9-427-2015>, 2015.

465 Global Soil Data Task: Global soil data products CD-ROM contents (IGBP-DIS), ORNL DAAC, 2014.

466 Gruber, S.: Derivation and analysis of a high-resolution estimate of global permafrost zonation, *The Cryosphere*, 6,
467 221–233, <https://doi.org/10.5194/tc-6-221-2012>, 2012.

468 Harden, J.W., Koven, C.D., Ping, C.-L., Hugelius, G., McGuire, A.D., Camill, P., Jorgenson, T., Kuhry, P.,
469 Michaelson, G.J., O’Donnell, J.A., Schuur, E.A.G., Tarnocai, C., Johnson, K. and Grosse, G.: Field information links
470 permafrost carbon to physical vulnerabilities of thawing. *Geophysical Research Letter*, 39, L15704,
471 <https://doi.org/10.1029/2012GL051958>, 2012.

472 Heiri, O., Lotter, A. F., and Lemcke, G.: Loss on ignition as a method for estimating organic carbon and carbonate
473 content in sediments: reproduction and comparability of results. *J. Paleolimnol.*, 25, 101–110,
474 <https://doi.org/10.1023/a:1008119611481>, 2001.

475 Hugelius G. and Kuhry, P.: Landscape partitioning and environmental gradient analyses of soil organic carbon in a
476 permafrost environment. *Global Biogeochem. Cycles*, 23, GB3006, <https://doi.org/10.1029/2008GB003419>, 2009.

477 Hugelius G., Kuhry, P., Tarnocai, C. and Virtanen, T.: Soil organic carbon pools in a periglacial landscape: a case
478 study from the central Canadian Arctic. *Permafrost Periglac. Process.*, 21: 16-29. <https://doi.org/10.1002/ppp.677>,
479 2010.

480 Hugelius, G., Virtanen, T., Kaverin, D., Pastukhov, A., Rivkin, F., Marchenko, S., Romanovsky, V. and Kuhry, P.:
481 High-resolution mapping of ecosystem carbon storage and potential effects of permafrost thaw in periglacial terrain,
482 European Russian Arctic, *J. Geophys. Res.*, 116, G03024, <https://doi.org/10.1029/2010JG001606>, 2011.

483 Hugelius, G.: Spatial upscaling using thematic maps: An analysis of uncertainties in permafrost soil carbon estimates.
484 *Global Biogeochem Cycles* GB2026. <https://doi.org/10.1029/2011GB004154>, 2012.

485 Hugelius, G., Bockheim, J. G., Camill, P., Elberling, B., Grosse, G., Harden, J. W., Johnson, K., Jorgenson, T., Koven,
486 C. D., Kuhry, P., Michaelson, G., Mishra, U., Palmtag, J., Ping, C.-L., O'Donnell, J., Schirrmeister, L., Schuur, E. A.
487 G., Sheng, Y., Smith, L. C., Strauss, J., and Yu, Z.: A new data set for estimating organic carbon storage to 3 m depth
488 in soils of the northern circumpolar permafrost region. *Earth Syst. Sci. Data*, 5, 393–402, [https://doi.org/10.5194/essd-](https://doi.org/10.5194/essd-5-393-2013)
489 5-393-2013, 2013.

490 Hugelius, G., Strauss, J., Zubrzycki, S., Harden, J. W., Schuur, E. A. G., Ping, C.-L., Schirrmeister, L., Grosse, G.,
491 Michaelson, G. J., Koven, C. D., O'Donnell, J. A., Elberling, B., Mishra, U., Camill, P., Yu, Z., Palmtag, J., and Kuhry,
492 P.: Estimated stocks of circumpolar permafrost carbon with quantified uncertainty ranges and identified data gaps.
493 *Biogeosciences* 11(23):6573– 6593, <https://doi.org/10.5194/bg-11-6573-2014>, 2014.

494 Hugelius, G., Loisel, J., Chadburn, S., Jackson, R.B., Jones, M., MacDonald, G., Marushchak, M., Olefeldt, D.,
495 Packalen, M., Siewert, M.B., Treat, C., Turetsky, M., Voigt, C. and Yu, Z.: Large stocks of peatland carbon and
496 nitrogen are vulnerable to permafrost thaw. *PNAS*, 117, 34, <https://doi.org/10.1073/pnas.1916387117>, 2020.

497 Köchy, M., Hiederer, R., and Freibauer, A.: Global distribution of soil organic carbon – Part 1: Masses and frequency
498 distributions of SOC stocks for the tropics, permafrost regions, wetlands, and the world, *SOIL*, 1, 351–365,
499 <https://doi.org/10.5194/soil-1-351-2015>, 2015.

500 Kracht, O and Gleixner, G.: Isotope analysis of pyrolysis products from Sphagnum peat and dissolved organic matter
501 from bog water. *Organic Geochemistry*, 31: 645–654, [https://doi.org/10.1016/S0146-6380\(00\)00041-3](https://doi.org/10.1016/S0146-6380(00)00041-3), 2020.

502 Kuhry, P. and Vitt, D.H.: Fossil Carbon/Nitrogen Ratios as a Measure of Peat Decomposition. *Ecology*, 77: 271-275.
503 <https://doi.org/10.2307/2265676>, 1996.

504 Kuhry, P., Mazhitova, G.G., Forest, P.-A., Deneva, S.V., Virtanen, T. and Kultti, S.: Upscaling soil organic carbon
505 estimates for the Usa Basin (Northeast European Russia) using GIS-based land cover and soil classification schemes.
506 *Geografisk Tidsskrift-Danish Journal of Geography*, 102:1, 11-25, <https://doi.org/10.1080/00167223.2002.10649462>,
507 2002.

508 McKinney, W.: "pandas: a foundational Python library for data analysis and statistics." Python for high performance
509 and scientific computing 14.9, 1-9, 2011.

510 Michaelson, G.J., Ping, C.-L. and Clark, M.: Soil Pedon Carbon and Nitrogen Data for Alaska: An Analysis and
511 Update. *Open Journal of Soil Science*, 2013, 3, 132-142 <http://dx.doi.org/10.4236/ojss.2013.32015>, 2013.

512 Mishra, U., Hugelius, G., Shelef, E., Yang, Y., Strauss, J., Lupachev, A., Harden, J.W., Jastrow, J.D., Ping, C.-L.,
513 Riley, W.J., Schuur, E.A.G., Matamala, R., Siewert, M., Nave, L.E., Koven, C.D., Fuchs, M., Palmtag, J., Kuhry, P.,
514 Treat, C.C., Zubrzycki, S., Hoffman, F.M., Elberling, B., Camill, P., Veremeeva, A. and Orr, A.: Spatial heterogeneity
515 and environmental predictors of permafrost region soil organic carbon stocks. *Science Advances*, 7, 9, [https://doi.org/](https://doi.org/10.1126/sciadv.aaz5236)
516 10.1126/sciadv.aaz5236, 2021.

517 Nachtergaele, F., van Velthuizen, H., Verelst, L., Batjes, N.H., Dijkshoorn, K., van Engelen, V.W.P., Fischer, G.,
518 Jones, A. and Montanarella, L.: The harmonized world soil database, in Proceedings of the 19th World Congress of
519 Soil Science, Soil Solutions for a Changing World, Brisbane, Australia, 1-6 August 2010, pp. 34–37, 2010.

520 National Wetlands Working Group. The Canadian Wetland Classification System, 2nd Edition. Warner, B.G. and
521 C.D.A. Rubec (eds.), Wetlands Research Centre, University of Waterloo, Waterloo, ON, Canada. 68 p, 1997.

522 Obu, J., Westermann, S., Bartsch, A., Berdnikov, N., Christiansen, H.H., Dashtseren, A., Delaloye, R., Elberling, B.,
523 Etzelmuller, B., Kholodov, A., Khomutov, A., Kääb, A., Leibman, M.O., Lewkowicz, A.G., Panda, S.K.,
524 Romanovsky, V., Way, R.G., Westergaard-Nielsen, A., Wu, T., Yamkhin, J. and Zou, D.: Northern Hemisphere
525 permafrost map based on TTOP modelling for 2000–2016 at 1 km² scale, *Earth-Science Reviews* 193,
526 <https://doi.org/10.1016/j.earscirev.2019.04.023>, 2019.

527 Obu, J.: How much of the Earth's surface is underlain by permafrost? *Journal of Geophysical Research: Earth Surface*,
528 126, e2021JF006123. <https://doi.org/10.1029/2021JF006123>, 2021

529 Oleson, K. W., Lawrence, D. M., Bonan, G.B., Flanner, M.G., Kluzek, E., Lawrence, P.J., Levis, S., Swenson, S.C.,
530 Thornton, P.E., Dai, A., Decker, M., Dickinson, R., Feddema, J., Heald, C.L., Hoffman, F., Lamarque, J.-F.,
531 Mahowald, N., Niu, G.-Y., Qian, T., Randerson, J., Running, S., Sakaguchi, K., Slater, A., Stockli, R., Wang, A.,
532 Yang, Z.-L., Zeng, X., and Zeng, X.: Technical description of version 4.0 of the Community Land Model (CLM),
533 2010.

534 Palmtag, J., Hugelius, G., Lashchinskiy, N., Tarmstorf, M.P., Richter, A., Elberling, B. and Kuhry, P.: Storage,
535 landscape distribution and burial history of soil organic matter in contrasting areas of continuous permafrost, *Arct.*
536 *Antarct. Alp. Res.*, 47, 71–88, <https://doi.org/10.1657/AAAR0014-027>, 2015.

537 Palmtag, J., Ramage, J., Hugelius, G., Gentsch, N., Lashchinskiy, N., Richter, A. and Kuhry, P.: Controls on the
538 storage of organic carbon in permafrost soils in northern Siberia, *Eur. J. Soil Sci.*, 67, 478–491,
539 <https://doi.org/10.1111/ejss.12357>, 2016.

540 Palmtag, J. and Kuhry, P.: Grain size controls on cryoturbation and soil organic carbon density in permafrost-affected
541 soils. *Permafrost and Periglac Process*, 29, <https://doi.org/10.1002/ppp.1975>, 2018.

542 Palmtag, J., Obu, J., Kuhry, P., Siewert, M., Weiss, N. and Hugelius, G.: Detailed pedon data on soil carbon and
543 nitrogen for the northern permafrost region. Dataset version 1. Bolin Centre Database.
544 <https://doi.org/10.17043/palmtag-2022-pedon-1>, 2022a.

545 Palmtag, J., Obu, J., Kuhry, P., Siewert, M., Weiss, N. and Hugelius, G.: A high spatial resolution soil carbon and
546 nitrogen dataset for the northern permafrost region. Dataset version 1. Bolin Centre Database.
547 <https://doi.org/10.17043/palmtag-2022-spatial-1>, 2022b.

548 Pascual, D., Kuhry, P. and Raudina, T.: Soil organic carbon storage in a mountain permafrost area of Central Asia
549 (High Altai, Russia). *Ambio*. <https://doi.org/10.1007/s13280-020-01433-6>, 2020.

550 Ping, C.L., Bockheim, J.G., Kimble, J.M., Michaelson J.J. and Walker, D.A.: Characteristics of cryogenic soils along
551 a latitudinal transect in arctic Alaska. *J. Geophys. Res.: Atmos.* 103, 917–928, <https://doi.org/10.1029/98JD02024>,
552 1998.

553 Pribyl, D. W.: A critical review of the conventional SOC to SOM conversion factor, *Geoderma*, 156(3), 75–83,
554 <https://doi.org/10.1016/j.geoderma.2010.02.003>, 2010.

555 Siewert, M.B., Hanisch, J., Weiss, N., Kuhry, P., Maximov, T.C. and Hugelius, G.: Comparing carbon storage of
556 Siberian tundra and taiga permafrost ecosystems at very high spatial resolution. *JGR - Biogeosciences*, Volume 120,
557 <https://doi.org/10.1002/2015JG002999>, 2015.

558 Siewert, M.B., Hugelius, G., Heim, B. and Faucherre, S.: Landscape controls and vertical variability of soil organic
559 carbon storage in permafrost-affected soils of the Lena River Delta. *CATENA*, Volume 147, Pages 725-741,
560 <https://doi.org/10.1016/j.catena.2016.07.048>, 2016.

561 Siewert, M. B.: High-resolution digital mapping of soil organic carbon in permafrost terrain using machine learning:
562 a case study in a sub-Arctic peatland environment, *Biogeosciences*, 15, 1663–1682, [https://doi.org/10.5194/bg-15-](https://doi.org/10.5194/bg-15-1663-2018)
563 1663-2018, 2018.

564 Siewert, M.B., Lantuit, H., Richter, A. and Hugelius, G.: Permafrost Causes Unique Fine-Scale Spatial Variability
565 Across Tundra Soils. *Global Biogeochemical Cycles*, 35, e2020GB006659. <https://doi.org/10.1029/2020GB006659>,
566 2021.

567 Strauss, J., Schirrmeister, L., Grosse, G., Fortier, D., Hugelius, G., Knoblauch, C., Romanovsky, V., Schädel, C.,
568 Schneider von Deimling, T., Schuur, T.A.G., Shmelev, D., Ulrich, M. and Veremeeva, A.: Deep Yedoma permafrost:
569 A synthesis of depositional characteristics and carbon vulnerability, *Earth-Science Reviews*, Volume 172,
570 <https://doi.org/10.1016/j.earscirev.2017.07.007>, 2017.

571 Thomson, S.K. Sampling. New York: John Wiley, 343 pp., 1992.

572 Turetsky, M.R., Abbott, B.W., Jones, M.C., Anthony, K.W., Olefeldt, D., Schuur, T.A.G., Koven, C., McGuire, A.D.,
573 Grosse, G., Kuhry, P., Hugelius, G., Lawrence, D.M., Gibson, C. and Sannel, A.B.K.: Permafrost collapse is
574 accelerating carbon release, *Nature*, 569, <https://doi.org/10.1038/d41586-019-01313-4>, 2019.

575 Weiss, N., Blok, D., Elberling, B., Hugelius, G., Jörgensen, C.J., Siewert, M.B. and Kuhry, P.: Thermokarst dynamics
576 and soil organic matter characteristics controlling initial carbon release from permafrost soils in the Siberian Yedoma
577 region. *Sedimentary Geology*, 340, 38-48, <https://doi.org/10.1016/j.sedgeo.2015.12.004>, 2016.

578 Weiss, N., Faucherre, S., Lampiris, N. and Wojcik, R.: Elevation-based upscaling of organic carbon stocks in High-
579 Arctic permafrost terrain: a storage and distribution assessment for Spitsbergen, Svalbard. *Polar Research*, 36,
580 <https://doi.org/10.1080/17518369.2017.1400363>, 2017.

581 Westermann, S., Schuler, T. V., Gislås, K. and Eitzelmüller, B.: Transient thermal modeling of permafrost conditions
582 in Southern Norway, *The Cryosphere*, 7, 719–739, <https://doi.org/10.5194/tc-7-719-2013>, 2013.

- 583 Westermann, S., Peter, M., Langer, M., Schwamborn, G., Schirrmeister, L., Eitzelmüller, B., and Boike, J.: Transient
584 modeling of the ground thermal conditions using satellite data in the Lena River delta, Siberia, *The Cryosphere*, 11,
585 1441–1463, doi.org/10.5194/tc-11-1441-2017, 2017.
- 586 Wojcik, R., Palmtag, J., Hugelius, G., Weiss, N. and Kuhry, P.: Landcover and landform-based upscaling of soil
587 organic carbon stocks on the Brøgger Peninsula, Svalbard, *Arctic, Antarctic, and Alpine Research*, 51:1, 40-57,
588 [https://doi.org/ 10.1080/15230430.2019.1570784](https://doi.org/10.1080/15230430.2019.1570784), 2019.